Acta Biomaterialia 163 (2023) 91–105

Contents lists available at ScienceDirect

Acta Biomaterialia

journal homepage: www.elsevier.com/locate/actbio

Full length article

Fascicular elastin within tendon contributes to the magnitude and modulus gradient of the elastic stress response across tendon type and species☆

Jeremy D. Eekhoff[a], James A. Abraham[b], Hayden R. Schott[b], Lorenzo F. Solon[c], Gabriella E. Ulloa[d], Jennifer A. Zellers[e], Paul C. Cannon[f], Spencer P. Lake[a,b,g,*]

[a] Department of Biomedical Engineering, Washington University in St. Louis, 1 Brookings Drive, MSC: 1185-208-125, St. Louis, MO 63130, United States
[b] Department of Mechanical Engineering and Materials Science, Washington University in St. Louis, United States
[c] Department of Biology, Washington University in St. Louis, United States
[d] Department of Mechanical Engineering, Massachusetts Institute of Technology, United States
[e] Department of Physical Therapy, Washington University in St. Louis School of Medicine, United States
[f] Department of Mathematics, Brigham Young University - Idaho, United States
[g] Department of Orthopaedic Surgery, Washington University in St. Louis School of Medicine, , United States

ARTICLE INFO

Article history:
Received 20 December 2021
Revised 7 March 2022
Accepted 10 March 2022
Available online 16 March 2022

Keywords:
Tendon
Elastin
Elastase
Elastic fibers
Fascicles

ABSTRACT

Elastin, the main component of elastic fibers, has been demonstrated to significantly influence tendon mechanics using both elastin degradation studies and elastinopathic mouse models. However, it remains unclear how prior results differ between species and functionally distinct tendons and, in particular, how results translate to human tendon. Differences in function between fascicular and interfascicular elastin are also yet to be fully elucidated. Therefore, this study evaluated the quantity, structure, and mechanical contribution of elastin in functionally distinct tendons across species. Tendons with an energy-storing function had slightly more elastin content than tendons with a positional function, and human tendon had at least twice the elastin content of other species. While distinctions in the organization of elastic fibers between fascicles and the interfascicular matrix were observed, differences in structural arrangement of the elastin network between species and tendon type were limited. Mechanical testing paired with enzyme-induced elastin degradation was used to evaluate the contribution of elastin to tendon mechanics. Across all tendons, elastin degradation affected the elastic stress response by decreasing stress values while increasing the modulus gradient of the stress-strain curve. Only the contributions of elastin to viscoelastic properties varied between tendon type and species, with human tendon and energy-storing tendon being more affected. These data suggest that fascicular elastic fibers contribute to the tensile mechanical response of tendon, likely by regulating collagen engagement under load. Results add to prior findings and provide evidence for a more mechanistic understanding of the role of elastic fibers in tendon.

Statement of significance

Elastin has previously been shown to influence the mechanical properties of tendon, and degraded or abnormal elastin networks caused by aging or disease may contribute to pain and an increased risk of injury. However, prior work has not fully determined how elastin contributes differently to tendons with varying functional demands, as well as within distinct regions of tendon. This study determined the effects of elastin degradation on the tensile elastic and viscoelastic responses of tendons with varying functional demands, hierarchical structures, and elastin content. Moreover, volumetric imaging and protein quantification were used to thoroughly characterize the elastin network in each distinct tendon. The

☆ Part of the Special Issue on the Mechanics of Cells and Fibers, guest-edited by Professors Amrinder S. Nain, Derrick Dean, and Guy M. Genin.

* Corresponding author at: Department of Biomedical Engineering, Washington University in St. Louis, 1 Brookings Drive, MSC: 1185-208-125, St. Louis, MO 63130, United States.
E-mail address: lake.s@wustl.edu (S.P. Lake).

https://doi.org/10.1016/j.actbio.2022.03.025

results presented herein can inform tendon-specific strategies to maintain or restore native properties in elastin-degraded tissue.

1. Introduction

Elastic fibers are an integral part of the extracellular matrix (ECM) of tendon. These elastic fibers are composite structures comprised of a scaffold of fibrillin-based microfibrils with a dense core of heavily cross-linked elastin [1]. Within fascicles – the largest hierarchical subunit of tendon – elastic fibers are relatively sparse and strongly aligned with the long axis of the tendon [2]. Conversely, elastic fibers located between fascicles in the interfascicular matrix (IFM) have been described as a denser mesh-like network [3,4].

Clinical trends suggest an important role for elastic fibers in maintaining healthy tendon function. Heritable disorders that affect elastic fibers such as Marfan syndrome, Williams-Beuren syndrome, and cutis laxa can cause changes to joint laxity, indicative of compromised mechanical integrity of the tendons and other connective tissues near the joint [5–8]. Furthermore, elastic fiber degradation during aging may be a cause for increased risk of tendon injury in the elderly population, possibly due to a loss of fatigue resistance [4,9–11].

It is hypothesized that elastin contributes to the mechanical properties of tendon by acting as a linking component between adjacent bundles of collagen and regulating collagen reorganization in response to loading [5]. Recent research using elastinopathic mouse models, either with reduced elastin content ($Eln^{+/-}$) or disconnected and globular elastic fiber nanostructure ($Fbln5^{-/-}$), has demonstrated that mouse tendon that develops without a normal elastic fiber network are stiffer than wild-type controls [12,13]. This effect is especially true of the Achilles tendon (AT) which has greater mechanical demands and is often classified as an energy-storing tendon, as opposed to positional tendons that experience lower strains during physiological loading [14]. Another technique that has been used to evaluate the contribution of elastic fibers to tissue mechanics is enzymatic treatment using elastase to break down elastin within the tissue; however, elastase-based studies have yielded inconsistent results. Some studies have reported changes to tendon and ligament tensile mechanics upon elastase treatment including decreased linear modulus, increased hysteresis, decreased failure stress, and increased transition strain, yet others reported no changes to these same properties [15–18]. The effect of elastase treatment on shear properties appears to be more pronounced; separate studies consistently reported decreased stress upon shear loading in tendon and ligament samples, which is governed most notably by sliding or shearing between tendon fascicles and fibers but also by rotation and shear within individual tendon sub-units [19,20]. Additionally, isolated tendon IFM displayed a considerable decrease in fatigue resistance upon elastase treatment [10].

Some of the seemingly conflicting results of these past studies may be accounted for by considering differences in experimental design, particularly in the ability to resolve subtle changes by normalizing data to account for sample variability. Still, much of what may appear to be contradictory results could potentially be resolved by considering which tendon was used in these elastase experiments. As mentioned previously, prior work using mouse models demonstrated a more substantial role for elastic fibers in energy-storing tendons compared to positional tendons [12]. Similarly, elastin content has been shown to be greater in energy-storing horse tendons than in positional tendons from the same limbs [4]. This information suggests that elastase treatment would have a larger impact on tendons with a more energy-storing function. In addition to differences between tendon types due to functional requirements, differences in tendon structure between different species could also lead to divergent responses to elastase. Smaller tendons from mice or rats lack the elastin-dense IFM that is present in tendons from larger animals and humans [21]. Because of the different distributions of elastic fibers within the IFM and within the fascicles of tendon, it is likely that interfascicular elastin and fascicular elastin function through different mechanisms. Consequently, elastase treatment of smaller tendon that lacks IFM may yield different results than larger tendon where the fascicular structure and IFM are both present.

Because of this variation in elastin content and distribution between different types of tendons, it is essential to account for tendon type in order to reach a comprehensive understanding of how elastic fibers affect tendon mechanics. Fully appreciating differences between tendons could also lead to progress in tendon-specific injury prevention and treatment. In this study, we sought to measure elastin content and distribution in a wide range of distinct tendons from various mammalian species and perform mechanical testing in conjunction with elastase treatment to evaluate the effect of elastin degradation on tensile mechanics of each tendon type. The study was designed to include samples that spanned a range of hierarchical organizations and functional demands.

2. Methods

2.1. Sample collection

Tendons were harvested from C57BL/6 mice (4-5 months, mixed sex), Long-Evans rats (4-5 months, male), mongrel dogs (2 years, female), duroc pigs (4-5 months, mixed sex), black angus cows (15–16 months, mixed sex), and humans (37–95 years, mixed sex). Due to the anatomical differences between these species, it has been proposed that the superficial digital flexor tendon (SDFT) and the long digital extensor tendon (LDET) of hooved mammals are functionally analogous to the Achilles tendon (AT) and the tibialis anterior tendon (TBAT), respectively, of humans and other non-hooved mammals [22]. Consequently, the SDFT and LDET were harvested from pig and cow hind limbs, and the AT and TBAT were harvested from mouse, rat, dog, and human limbs as representative energy-storing and positional tendons, respectively, that can be compared between species.

Mouse tendons were either harvested immediately after euthanasia and flash frozen in optimal cutting temperature compound (OCT) for two-photon microscopy or stored at –20 °C until later use for compositional analysis or mechanical testing. Rat and dog tendons were harvested from animals used in other studies and stored at –20 °C. Pig and cow hind limbs, purchased from a local abattoir, were harvested immediately and flash frozen in OCT for two-photon microscopy or stored at –20 °C until later use for compositional analysis or mechanical testing. Human tendons used for compositional analysis and mechanical testing were acquired through anatomical donations at the Washington University in St. Louis School of Medicine (age range 79–95 years). Separate human tendon samples used for two-photon microscopy were freshly harvested from individuals undergoing below knee amputation; small pieces of tendon (~1 cm^3) were immediately flash frozen in OCT

for two-photon microscopy (age range 37–63 years). The cause of amputation was failure of prior orthopaedic surgery, complications from trauma, osteomyelitis, or Charcot foot deformity. All tendon tissue appeared visually normal with no evidence of disease or damage.

All experiments were performed with approval from the Institutional Animal Care and Use Committee and the Institutional Review Board.

2.2. Compositional analysis

Energy-storing and positional tendons from all six species were used for compositional analyses as described previously (n = 4–6 per group) [23]. Briefly, a segment of the tendon midsubstance was isolated and weight was recorded before and after lyophilization. Samples were hydrolyzed in 6N hydrochloric acid at 100 °C for 48 h, dried, and rehydrated in water.

Collagen content was measured using a Chloramine-T and Erlich's solution colorimetric assay using a standard curve of pure hydroxyproline, assuming collagen contains 13.5% hydroxyproline by mass [23]. Elastin content was measured using a competitive enzyme-linked immunosorbent assay with an anti-desmosine antibody measured using a standard curve of purified elastin, assuming the ratio of desmosine to elastin was consistent between all samples and the elastin used for the standard curve.

Tendon composition data were analyzed using a linear mixed model that included species, tendon type (i.e., energy-storing vs. positional), and the species-tendon type interaction as fixed effects, and included donor as a random effect. Post-hoc comparisons of predicted means with Bonferroni correction were performed within significant highest-order fixed model effects.

Based on results from elastin content determination (see Results section), tendons from mouse, cow, and human were selected for further analysis.

2.3. Two-photon microscopy

Three-dimensional image stacks of elastin, collagen, and cell nuclei in energy-storing and positional mouse, cow and human tendons were acquired using two-photon microscopy (n = 5 per group).

Mouse tendons were freshly harvested and immediately flash frozen in OCT. The tendons were transversely sectioned using a cryostat to a thickness of 150 µm. After rinsing the sections in 0.1X PBS for 5 min three times to clear the OCT, sections were incubated in 16 µM Alexa Fluor 633 Hydrazide and 8 µg/mL Hoechst 33342 in a blocking solution of 1% bovine serum albumin and 0.05% Triton-X in 0.1X PBS for 2 h to fluorescently label elastin and cell nuclei, respectively [24]. Sections were then rinsed an additional three times in 0.1X PBS for 5 min each.

Small pieces (~1 cm^3) of cow and human tendons that were freshly harvested were immediately flash frozen in OCT. A cryostat was used to remove tissue from opposite ends of the sample in a transverse orientation. Subsequently, samples were rinsed in PBS, incubated in 2 µM Alexa Fluor 633 Hydrazide and 1 µg/mL Hoechst 33342 in the blocking solution described above to fluorescently label elastin and cell nuclei, respectively [24]. Samples were incubated in serial solutions of 30% fructose, 60% fructose, and 90% fructose with 0.5% α-thioglycerol in 0.1X PBS for 2 h each and then left in the 90% solution overnight to optically clear the tissue [25].

Three-dimensional (3D) image stacks were acquired using a two-photon microscope. Collagen was imaged using second harmonic generation (excitation 1200 nm; emission 595–605 nm), while elastin and cell nuclei were fluorescently imaged using the labels listed above (excitation 810nm; emission 640–660 nm and 440–500 nm, respectively). Two image stacks were acquired at randomly selected locations from the cow and human tendon samples. Because the mouse tendon sections were mostly captured within a single field of view, only one image stack was acquired per mouse tendon sample.

Regions of IFM and fascicular matrix (FM) in the image stacks were separated using manual tracing of the collagen signal without knowledge of the elastin or cell nuclei signals to avoid bias in the tracing. Elastic fibers were isolated from background signal in the elastin channel using background subtraction and automated intensity thresholding. Similarly, cell nuclei were isolated using automated thresholding. The elastic fiber network was analyzed using a voxel-wise 3D fiber analysis algorithm to calculate fiber orientation and connectivity [26]. For cow and human image stacks, the voxel-wise data were combined across the two acquired images to compute average values for each tendon sample.

Quantitative data from two-photon microscopy were analyzed using a linear mixed model that included species, tendon type, region (i.e., FM vs. IFM), the species by tendon type interaction, and the tendon type by region interaction as fixed effects, and included donor as a random effect. The interaction between species and region and the three-way interaction between species, region, and tendon type were not included because mouse tendon lacked data across both regions, making it impossible to analyze these effects while including the entire dataset. Post-hoc comparisons of predicted means with Bonferroni correction were performed within significant highest-order fixed model effects.

2.4. Elastase verification

Mouse AT and cow SDFT were used to confirm elastin degradation upon exposure to elastase (n = 3–4 per group). Mouse ATs were isolated and clamped on opposite ends to simulate conditions for mechanical testing, then incubated in a control solution containing 0.1 mg/mL soybean trypsin inhibitor (Elastin Products Co., SB903) in 1X PBS or an elastase solution containing 0.1 mg/mL of soybean trypsin inhibitor and 4.0 units/mL of porcine pancreatic elastase (Elastin Products Co., EC134) in 1X PBS for 2 h at 37 °C, where one unit of elastase is the quantity able to hydrolyze 1 µmol of the substrate Suc-$(Ala)_3$-p-nitroanilide (Elastin Products Co., NS945) in one minute under the conditions described previously [27]. Similarly, 90 mm-long segments from the midsubstance of cow SDFTs were isolated and the ends were wrapped in latex and clamped to simulate conditions for mechanical testing. The SDFT segments were incubated in the same elastase solution or control solution for 24 h at 37 °C.

Following incubation, tendons were flash frozen in OCT and transversely sectioned to a thickness of 80 µm. The tendon sections were imaged using a two-photon microscope using a 25 X/0.95 NA water immersion lens. Images were taken of the cow SDFT at 1 mm increments from the edge of the tendon; the mouse AT cross-section was largely contained within a single field of view. Elastin was imaged using two-photon excited autofluorescence (excitation 880 nm; emission 495–540 nm) and collagen was imaged using second harmonic generation (excitation 880 nm; emission 400–440 nm). The elastin was isolated from the background autofluorescence using background subtraction and automated thresholding, and the volume ratio of elastin to collagen in each image was calculated using an intensity threshold to determine collagen volume.

Elastase verification data were analyzed using linear mixed models. Mouse data included treatment as a fixed effect and donor as a random effect. Cow data included treatment, distance from tendon edge, and their interaction as fixed effects, with donor included as a random effect. Post-hoc comparisons of predicted

means with Bonferroni correction were performed within significant highest-order fixed model effects.

2.5. Mechanical testing

Mechanical testing was performed on energy-storing and positional tendons from mice, cows, and humans before and after incubation in either elastase or control solution, described above (n = 5–7 per group). Testing using incubation in control solution was necessary to account for changes to mechanical properties that result from repeated mechanical testing and from extended incubation periods. Using this approach, data can be normalized within samples to the pre-incubation properties, and can also be normalized between treatment groups (i.e., without or with elastase) to fully isolate the effects of elastin degradation on tendon mechanics.

Mouse tendons were isolated from surrounding tissue and cross-sectional area (CSA) was measured using a laser scanning device. Samples were clamped between pieces of sandpaper to prevent slipping in a custom fixture. After loading the fixture in the test machine and establishing a pre-stress of 0.5 MPa, samples were subjected to a mechanical test consisting of ten cycles of preconditioning to 6% strain at a rate of 1 %/s, 10 min of stress relaxation at 6% strain, and three triangular loading curves to 2, 4, and 6% strain at a rate of 1 %/s, with one minute of rest between each segment of the test. After the initial test, the clamp fixture was removed and incubated in either control or elastase solution as described above while maintaining the gauge length at 37 °C for 2 h. The samples were re-tested following the incubation using the test protocol described above.

Cow and human tendons were cut to a length of 90 mm and thinned to a thickness of 1.5–2.0 mm using a freezing stage microtome to improve clamping and to ensure complete penetration of elastase into the samples (see Results section). After samples were thinned, CSA was measured using a laser scanning device. The central 40 mm of each sample was wrapped in PBS soaked gauze while the ends were left exposed, and the sample was placed in a room at 37 °C for 1.5 h to dry the tendon ends for improved clamping. Samples were then clamped between pieces of sandpaper in a custom clamping fixture, and clamps were sealed with putty to prevent rehydration of the tendon ends. After loading the fixture in the testing machine and establishing a pre-stress of 0.5 MPa, samples were mechanically tested using the same protocol listed above for mouse tendon, incubated in either control or elastase solution as described above at 37 °C for 24 h, and then re-tested using the same protocol.

For all tests using elastase, the activity of the solution against the substrate Suc-$(Ala)_3$-p-nitroanilide was monitored daily by measuring the rate of change of absorbance at 410 nm during the initial reaction between the elastase solution and substrate to ensure consistency between tests [27]. When the activity as defined above dropped below 3.6 units/mL, additional elastase was added to return the activity to 4.0 units/mL.

Stress relaxation data were analyzed using quasi-linear viscoelastic (QLV) theory, where the stress relaxation response over time is given by the convolution integral of the reduced relaxation function ($G(t)$) with the instantaneous elastic stress response ($\sigma^e(\varepsilon)$) [28]. The forms of the instantaneous elastic stress response and the reduced relaxation function used in this study are given in Eqs. (1) and (2), respectively [29–31].

$$\sigma^e(\varepsilon) = A\left(e^{B\varepsilon} - 1\right) \tag{1}$$

$$G(t) = \frac{1 + C[E_1(t/\tau_2) - E_1(t/\tau_1)]}{1 + C\ln(\tau_2/\tau_1)} \tag{2}$$

The material constants A and B describe the magnitude and nonlinearity of the elastic stress response, respectively, the material constant C describes the shape of the relaxation function, τ_1 and τ_2 are the relaxation time constants, and E_1 is the exponential integral function. The QLV model was fit to the ramp and relaxation data to determine these five material constants for each sample (Fig. 1(a, b)). Details on the model fitting are included in Appendix A [32].

Hysteresis values were calculated from the three triangular loading waveforms to 2, 4, and 6% strain as the difference between the integrals of the loading and unloading curves divided by the integral of the loading curve. The modulus was determined through a linear regression fit to the data from the final 0.5% strain of the ramp to 6% strain. The transition point between the toe and linear region was determined from the intersection of the loading curve and a parallel line offset by 0.5% from the regression modulus line (Fig. 1(c)).

To ensure that the samples used across the control and elastase treatment groups had similar baseline mechanics, the pre-incubation mechanical properties from tendons within each subgroup of species and tendon type were analyzed using a linear mixed model with treatment as a fixed effect and donor as a random effect.

To compare baseline properties across species and tendon time, pre-incubation mechanical properties were analyzed using a linear mixed model with species, tendon type, and their interaction as fixed effects, and donor as a random effect. Post-hoc comparisons of predicted means with Bonferroni correction were performed within significant highest-order fixed model effects. These data and the corresponding analysis are included in Appendix B.

Finally, mechanical data were analyzed to evaluate the effects of elastase on mechanical properties. All data were normalized within each sample by subtracting the post-incubation measurements from the pre-incubation measurements (Fig. 2(a, b)). The magnitude differences between pre- and post-incubation measurements were evaluated as opposed to the percent differences because while neither can be properly assumed to fully account for inter-sample variability, magnitude differences provide real, dimensioned quantities with more meaning than dimensionless percent values and also produce more consistent data for material constants with small values where percent differences can be considerably large. Within the control groups, these magnitude difference values represent the effect of repeated mechanical testing, while in the elastase groups, these values represent the sum of the effect of repeated mechanical testing and the effect of elastase treatment. These normalized data were analyzed using a linear mixed model that included species, tendon type, treatment and all possible interactions as fixed effects and included donor as a random effect. Additionally, the pre-incubation values for each measurement were included as a fixed effect to account for initial variability between individual samples within groups. For each group, the difference between the least squares means of the control and elastase groups along with the standard error of that difference were calculated to determine the isolated effect of elastase treatment on each mechanical property (Fig. 2(b, c)). Where warranted by the model fixed effects, post-hoc testing of the isolated effects of elastase with Bonferroni corrections was performed to determine (1) if the isolated effect of elastase was significant (i.e., different than zero) and (2) if the isolated effect of elastase varied by species and/or tendon type. Fixed effects not including treatment were necessary for model fitting, but their significance was not relevant to this study so they were not evaluated further regardless of significance.

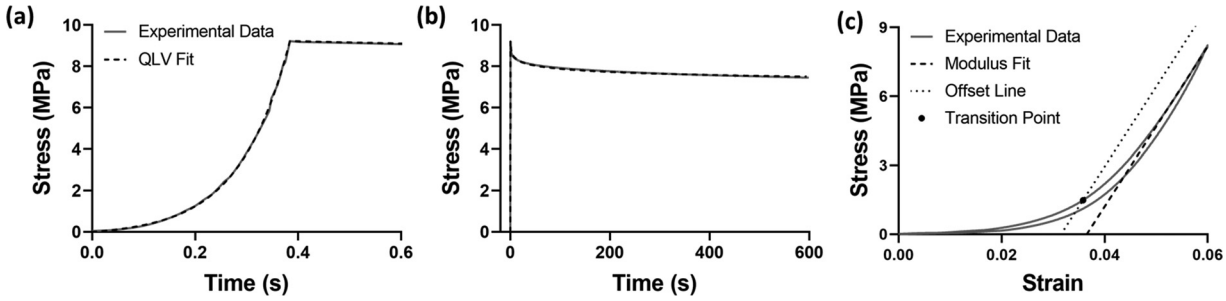

Fig. 1. Analysis of mechanical testing data. Representative QLV fitting to the (a) ramp and (b) relaxation portions of stress relaxation. (c) Hysteresis is calculated from the integrals of the loading and unloading curves. The modulus is determined by linear regression to the final 0.5% strain of the loading curve, while the transition stress and strain are calculated from the intersection of a parallel line offset by 0.5% strain from the fit modulus line with the loading curve.

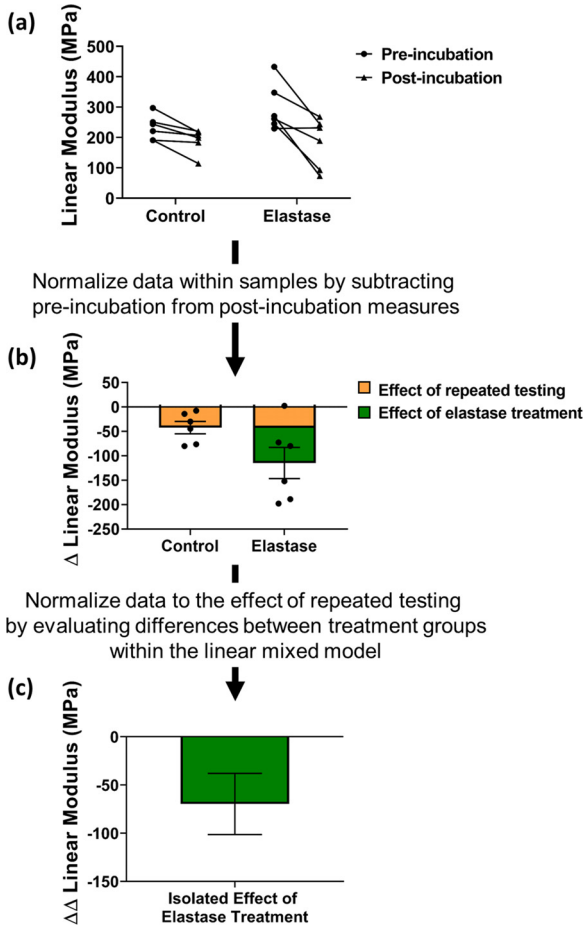

Fig. 2. Statistical modeling is used to isolate the effects of elastin degradation on tendon mechanics. (a) Raw experimental data has two values from each sample. (b) Data are normalized within samples by subtracting the pre-incubation value from the post-incubation value. These data are input into a linear mixed model. (c) To normalize data to the effect of repeated mechanical testing shown in the control treatment group, the difference between treatment groups is determined within the linear mixed model, which includes data across species and tendon types (not shown in this figure).

2.6. Statistical analyses

All statistical analyses described above were performed using JMP (SAS Institute). Due to the nature of this study, where a large number of groups were analyzed with relatively small sample sizes, *p*-values less than 0.10 were considered statistically significant to decrease the potential for false negatives, while individual *p*-values for each effect were independently considered in data analysis and interpretation [33,34]. Fixed effect *p*-values are included in the figures while post-hoc comparison *p*-values are represented with symbols. Plots were produced using Prism (GraphPad). All data bars are shown as mean ± standard error. Mean values described in the results section below represent the least squares means from model predictions.

3. Results

3.1. Tendon composition

The effect of tendon type on collagen content (Fig. 3(a)) normalized to dry weight was dependent on species (i.e., significant species*tendon type fixed effect). Post-hoc comparisons were used to determine which species had significant differences between tendon types. In mice, energy-storing tendons had higher collagen content than positional tendons. Conversely, pig and cow positional tendons had higher collagen content than energy-storing tendons. Collagen content was similar between tendon types in rat, dog, and human tendons.

Elastin content normalized to dry weight was 16% greater in energy-storing tendons compared to positional tendon, with mean values of 1.01% and 0.87% across all species, respectively (Fig. 3(b)). Moreover, elastin content varied by species. Most notably, human tendons had more elastin than all other species by a factor of two or more. Other, smaller differences between elastin content in other species were also statistically significant: cow vs. pig, cow vs. rat, dog vs. pig, and mouse vs. pig.

Based on these results, tendons from mice (lower elastin content and no IFM), cow (lower elastin content with IFM), and human (higher elastin content with IFM) were chosen for further experimentation to represent a range of elastin contents and structural hierarchies.

3.2. Tendon structure and elastin distribution

Two-photon microscopy produced clear 3D images of collagen, elastic fibers, and cell nuclei (Fig. 4). Distinct collagen fascicles were evident in the cross-sections of cow and human tendon, although the IFM was visually more distinct in human tendon compared to cow. Mouse tendon appeared similar to a single fascicle from cow or human tendon and did not contain any noticeable IFM. Individual elastic fibers could be distinguished within the elastin channel of the image stacks, where the fibers were generally straight and aligned with the major axis of the tendon (Fig. 4(g–l)). Elastic fibers within the IFM of cow and human tendon appeared qualitatively more densely packed and less organized compared to elastic fibers in the FM.

Within the two-photon microscopy image stacks, the mean cellular density was approximately four-fold greater in the IFM com-

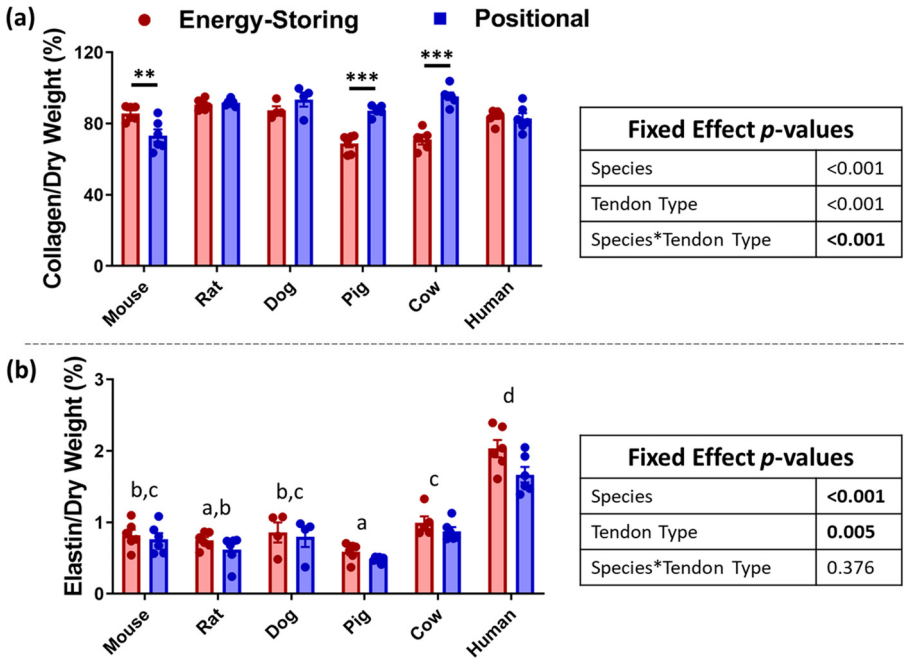

Fig. 3. (a) The effect of tendon type on collagen content was dependent on species. Energy-storing tendons had greater collagen content compared to positional tendons in mice, while positional tendons had greater collagen content compared to energy-storing tendons in pig and cow. $^{**}p < 0.01$, $^{***}p < 0.001$ (b) Elastin content was greater in energy-storing tendons compared to positional tendon across all species. Human tendon had at least double the elastin content compared to other species, and there were other, smaller differences between species. Different letters indicate a significant ($p < 0.1$) difference between species.

pared to the FM but was not significantly affected by tendon type or species (Fig. 5(a)).

Analysis of the isolated elastic fiber network yielded measurements of volume ratio, connectivity ratio, and orientation variance [26]. The effect of tendon region on elastin volume (Fig. 5(b)) was dependent on tendon type (i.e., significant tendon type*region fixed effect). While the volume ratio was greater in the IFM compared to FM of both tendon types, the effect only reached significance in energy-storing tendons with post-hoc testing, while the effect in positional tendons was statistically insignificant. Similarly, the elastin volume ratio was generally greater in energy-storing tendons compared to positional tendons, but the effect was statistically significant in the IFM but not the FM. Species had no significant impact on elastin volume measured in the two-photon microscopy images, although general trends were similar to the differences observed in the compositional analysis reported above.

The connectivity ratio output by the fiber analysis algorithm provides a measure between zero and one, indicating the ratio of voxels that are part of a fiber intersection or branching location. The elastic fiber network was determined to be more connected in the IFM compared to the FM (Fig. 5(c)). Furthermore, the effect of tendon type on connectivity was dependent on species (i.e., significant species*tendon type fixed effect). In cow, energy-storing tendons had greater elastic fiber connectivity than positional tendons, while tendon type did not significantly impact connectivity in mouse and human tendon. Within this interaction, there was also a significant difference between cow and human positional tendons where the human positional tendons had greater connectivity.

Lastly, the orientation variance was calculated from the three-dimensional orientation distribution (Fig. 5(d)). This measurement gives a value between zero and one, where zero indicates perfect alignment and one represents fully isotropic alignment. The variance was higher (i.e., the elastic fibers were less aligned) in the IFM compared to the FM, with mean values of 0.27 and 0.11 across species, respectively. Although the variance in orientation was greater in the IFM, the relatively low value of 0.27 indicates the elastic fibers in the IFM still demonstrate a dominant orientation along the axis of the tendon, although less strongly than in the FM. Orientation variance was also different between species: cow tendon had lower variance values than both mouse and human tendon.

In summary, the largest effects in cell quantity and elastin structural organization were seen in differences between the IFM and FM. Compared to the FM, the IFM had greater cellular density and a denser, more connected, and less aligned elastic fiber network. Smaller effects were observed between species and tendon type, where larger differences were observed in fiber connectivity and diameter between tendon types in cow tendon compared to mouse and human tendon. Although the interaction between species and region could not be evaluated due to mouse tendon lacking IFM, there were larger differences between IFM and FM in human tendon compared to cow tendon, and the IFM qualitatively appeared more distinct in human tendon.

3.3. Elastase verification

Degradation of elastin with elastase treatment was demonstrated using two-photon excited autofluorescent imaging of elastin, where the elastin signal was significantly diminished after enzymatic treatment. In mouse Achilles tendon, elastin signal was decreased by 80% throughout the whole cross-section of the tendon (Fig. 6(a)). In contrast, the effectiveness of elastase treatment was dependent on location in cow tendon due to the larger size (Fig. 6(b)). Elastin volume in control images was not dependent on location, so these data were pooled together for comparison to elastase-treated tendon. From the periphery of the tendon up to 2 mm from the tendon edge, elastin was significantly degraded. However, the elastin content was unaffected further towards the center of the tendon after the 24 h incubation, indicating that the

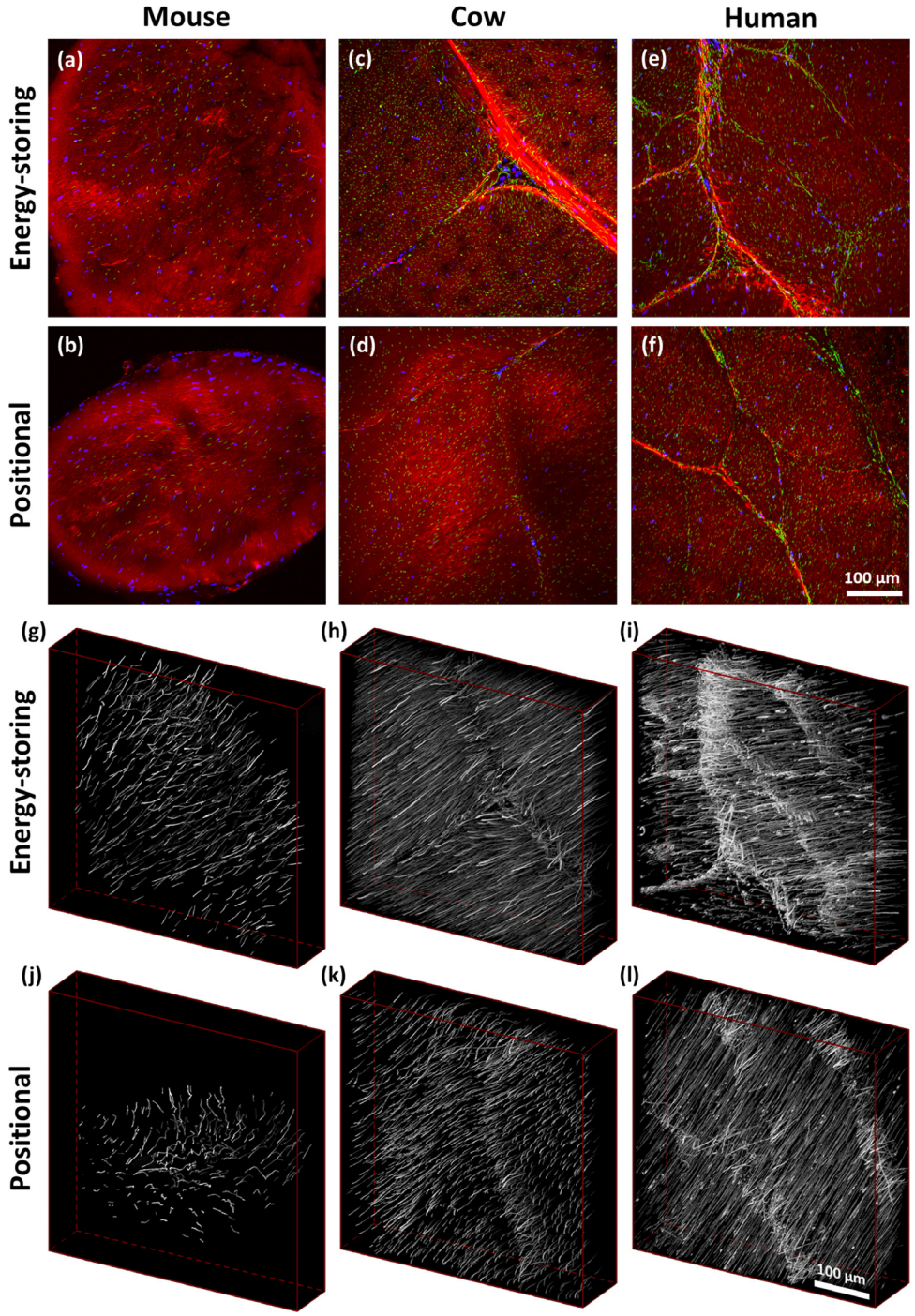

Fig. 4. Representative two-photon microscopy images of tendon cross-sections across species and tendon types. (a–f) Maximum intensity projections across a depth of 5 µm showing collagen (SHG) in red, elastin (Alexa 633) in green, and cell nuclei (Hoechst 33342) in blue. (g–l) Three-dimensional reconstructions of the elastic fiber network from the full image stack.

elastase enzyme only penetrated 2 mm-deep into the sample. Consequently, all samples for mechanical testing were thinned to a maximum thickness of 2 mm to ensure complete elastin degradation. With both sides of the tendon exposed to the elastase solution, this incorporated a sufficient safety factor to have confidence in the elastase treatment protocol.

3.4. Effect of elastase on mechanical properties

Comparison of pre-incubation mechanical properties between tendons designated to control or elastase treatment groups was performed to ensure baseline differences in mechanical properties did not affect subsequent measurements and analyses. Of all properties measured, the only statistically significant difference in baseline properties between treatment groups was the modulus of cow energy-storing tendons (data not shown). This difference was considered to be acceptable because of (1) relatively low significance ($p = 0.053$), (2) no other material constants had a statistically significant difference between these groups, and (3) subsequent analyses did not reveal any unusual results to indicate that the minor difference in baseline properties impacted any conclusions from the data.

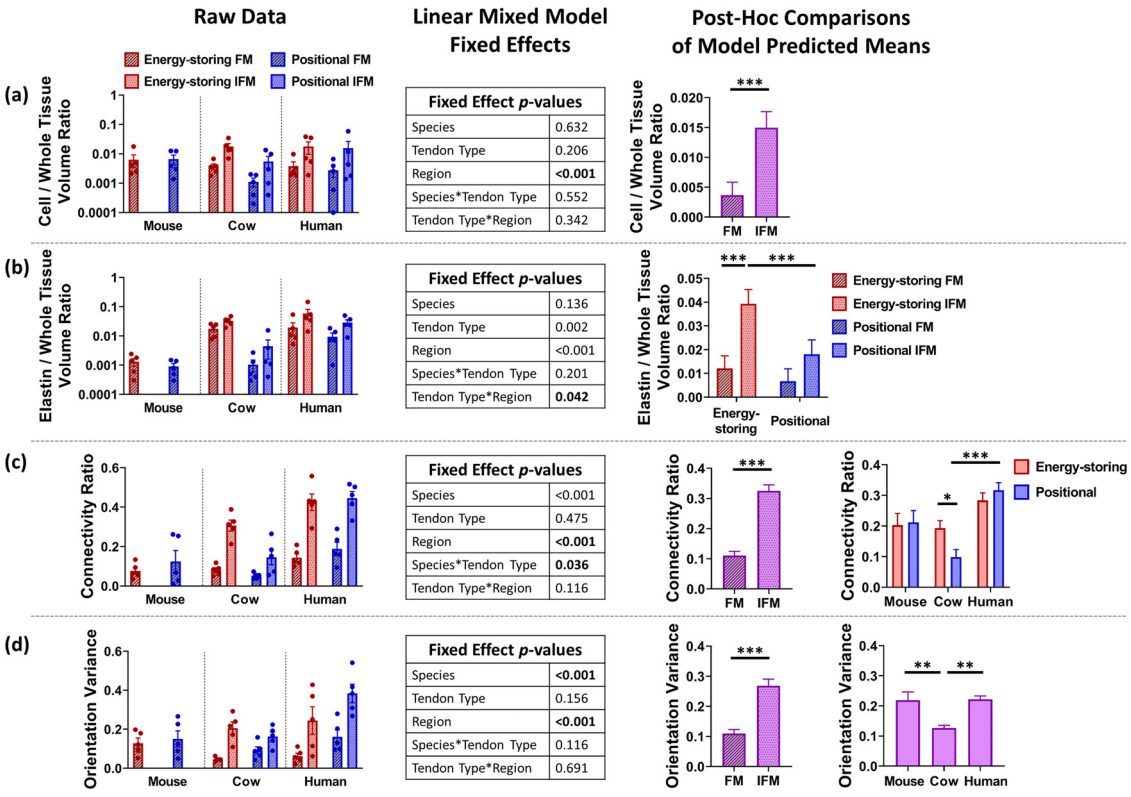

Fig. 5. Data and statistical analysis from two-photon microscopy. Post-hoc testing was performed only within significant highest order fixed effects, with *p*-values shown in bolded font. (a) The IFM had a four-fold greater volume of cell nuclei compared to the FM without distinction between species or tendon type. (b) The effect of region on elastin volume was dependent on tendon type. Energy-storing IFM had greater elastin volume than energy-storing FM and positional IFM. (c) Connectivity of the elastic fiber network was greater in the IFM than the FM across species and tendon types. The effect of tendon type on elastic fiber connectivity was dependent on species, where cow positional tendon has lesser connectivity compared to cow energy-storing tendon and human positional tendon. (d) Elastic fibers in the FM were more aligned than elastic fibers in the IFM across all species and tendon types, and elastic fibers in cow tendon were more aligned than elastic fibers in mouse or human tendon independent of region or tendon type. $^{**}p<0.01$, $^{***}p < 0.001$.

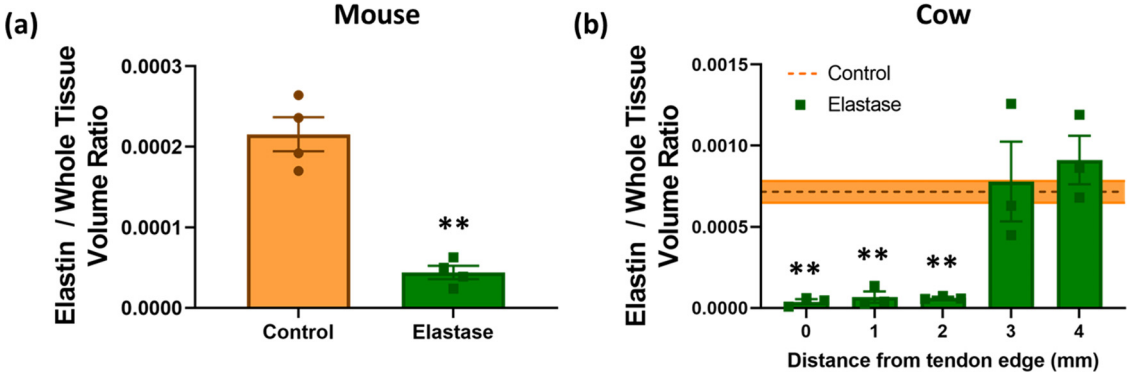

Fig. 6. (a) Elastase treatment significantly degraded elastin through mouse tendon. (b) Elastase treatment significantly degraded elastin in cow tendon up to 2 mm from the tendon edge, while deeper into the tendon was not affected. $^{**}p < 0.01$.

A detailed comparison of the effects of species and tendon type on baseline mechanical properties is outside of the main focus of this study (namely, the effect of elastin removal on subsequent properties). Still, the analysis was performed and results are included in Appendix B.

The QLV theory produced good fits for all experimental data and yielded five material constants for each sample: *A, B, C,* τ_1, and τ_2. The first two constants, *A* and *B*, are primarily indicative of elastic properties. The change in the constant *A*, which represents the magnitude of the stress response, was decreased by elastase treatment in comparison to control treatment by an average of 0.19 MPa, demonstrating an overall effect of elastase across all tendons (Fig. 7(a)). The material constant *B* primarily indicates the shape, or the modulus gradient, of the loading curve, where a higher value of *B* signifies a curve in which the rate of increase of the tangent modulus with increasing strain is increased. Elastase treatment sig-

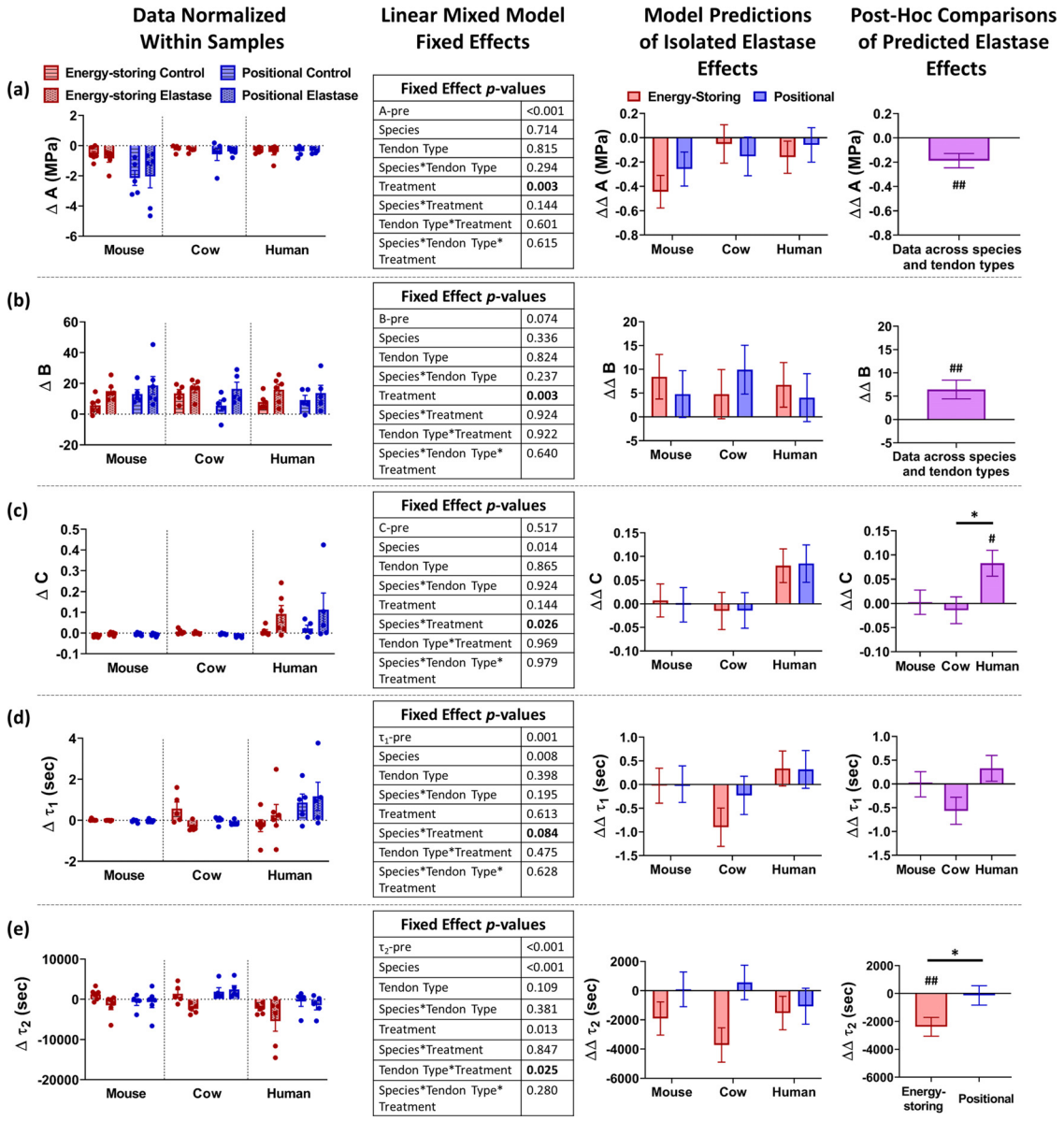

Fig. 7. Data and statistical analysis from QLV fitting of stress relaxation. Model predictions of isolated elastase effects are the difference between treatment groups for each tendon group. Post-hoc testing was performed only within significant highest order fixed effects that included treatment, with *p*-values shown in bolded font. (a) The constant *A* was decreased by elastase treatment across all species or tendon types. (b) The constant *B* was increased by elastase treatment across all species and tendon types. (c) The effect of elastase treatment on *C* was dependent on species, where *C* was significantly increased by elastase treatment in human tendon but not mouse or cow tendon independent of tendon type. (d) The effect of elastase treatment on τ_1 was dependent on species, although the effect on any individual species was not significant. (e) The effect of elastase treatment on τ_2 was dependent on tendon type, where τ_2 was decreased by elastase in energy-storing tendon but not positional tendons independent of species. Individual bars significantly different than zero: $^{\#}p < 0.1$, $^{\#\#}p < 0.01$. Significant difference between bars: $^{*}p < 0.1$.

nificantly increased *B* across all species and tendon types by an average of 6.46, indicating an increased modulus gradient caused by the removal of elastin (Fig. 7(b)).

The effect of elastase on the material constant *C* (Fig. 7(c)), which represents the shape of the relaxation curve, was dependent on species (i.e., significant species*treatment fixed effect). In both human tendon types, *C* was significantly increased upon exposure to elastase, while cow and mouse tendon values of *C* were not affected. The change in the fast relaxation time constant τ_1 was dependent on the interaction between species and treatment (Fig. 7(d)). However, this effect had relatively low significance and post-hoc testing of the isolated elastase effects on individual species showed no significant differences. The slow relaxation time constant τ_2 (Fig. 7(e)) was significantly decreased after elastin degradation in energy-storing tendons compared to controls but was unaffected by elastase in positional tendons (i.e., significant tendon type*treatment fixed effect).

Hysteresis at lower strains was variable due to low signal-to-noise ratios in the stress data, so only hysteresis values calculated from the 6% strain curves are reported. The effect of elastase treatment on hysteresis (Fig. 8(a)) was dependent on the interaction between species and tendon type (i.e., significant species*tendon type*treatment fixed effect). Of all tendons used in this study, only mouse energy-storing tendons demonstrated a statistically significant effect of elastase treatment on hysteresis, with increased values after elastin degradation. The effects of elastase in cow and hu-

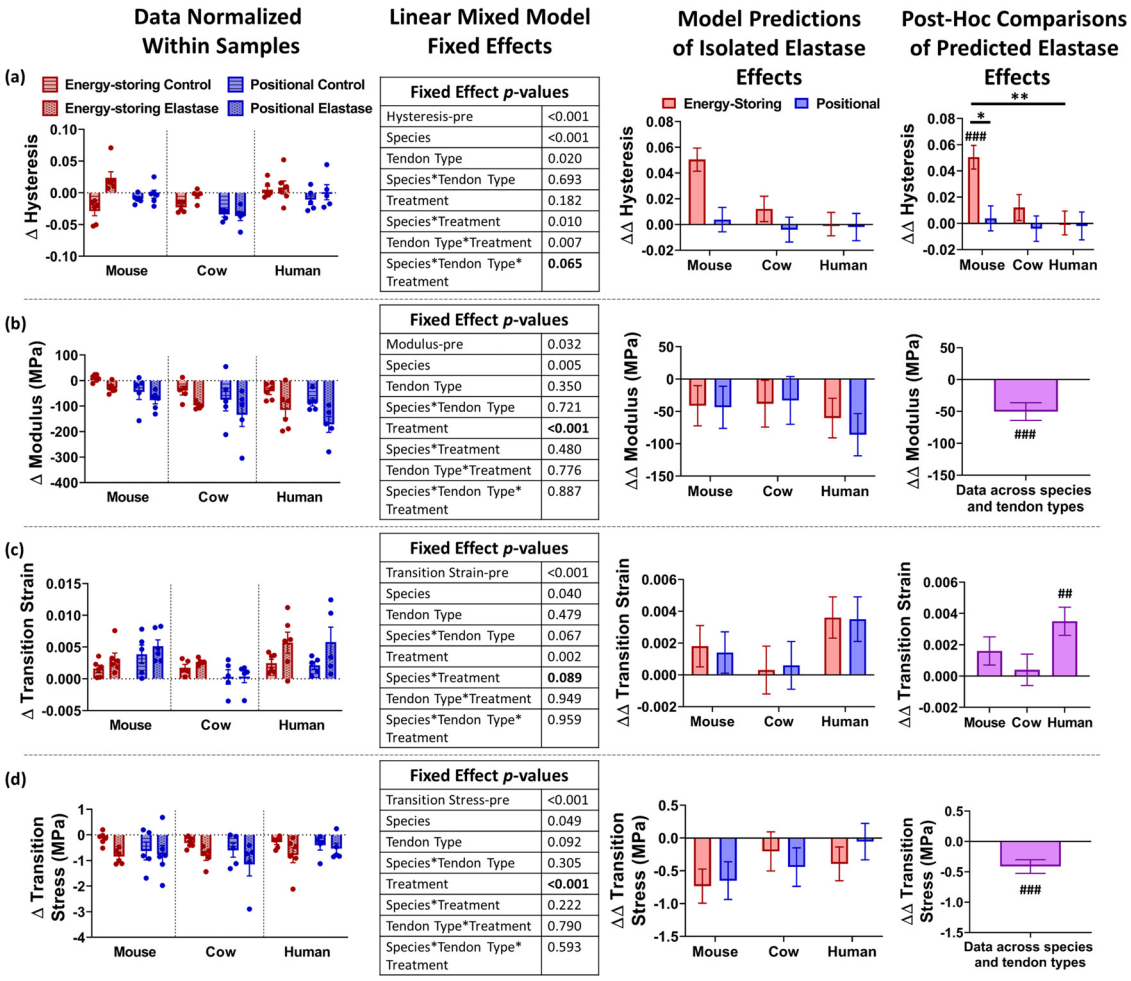

Fig. 8. Data and statistical analysis from hysteresis curves. Model predictions of isolated elastase effects are the difference between treatment groups for each tendon group. Post-hoc testing was performed only within significant highest order fixed effects that included treatment, with p-values shown in bolded font. (a) The effect of elastase treatment on hysteresis was dependent on the interaction between species and tendon type. Energy-storing mouse tendon had elevated hysteresis as a result of elastase compared to positional mouse tendon and energy-storing human tendon. (b) Tendon modulus was decreased by elastase treatment across all species and tendon types. (c) The effect of elastase treatment on transition strain was dependent on tendon species, where elastase increased transition strain in human tendon independent of tendon type. (d) Transition stress was decreased by elastase treatment across all species and tendon types. Individual bars significantly different than zero: $^{\#\#}p < 0.01$, $^{\#\#\#}p < 0.001$. Significant difference between bars: $^{*}p < 0.1$, $^{**}p < 0.01$.

man tendon were not significant and were not different between tendon types in these species.

Modulus values were significantly affected by treatment with an average decrease of 50 MPa resulting from elastin degradation across all tendons (Fig. 8(b)). In addition, the measured transition point of the stress-strain curve was shifted due to elastase treatment. Transition strain (Fig. 8(c)) increased more after elastase treatment in comparison to controls, although the effect was only significant in human tendon (i.e., significant species*treatment fixed effect). Lastly, transition stress was decreased by an average of 0.4 MPa across all tendons after elastase treatment (Fig. 8(d)).

4. Discussion

The results reported herein highlight the importance of elastic fibers in tendon, demonstrating that elastin and elastic fibers are an integral part of the tendon structure and contribute significantly to its mechanical function. While these data suggest that elastic fibers meaningfully impact all types of tendons, some are more affected by elastic fibers than others. Acknowledging the distinctions between tendons can improve the ability to interpret and translate results between scientific studies that utilize different tendon models, and more importantly, can ultimately lead to tendon-specific treatments for injury or degeneration that can more fully restore the native properties of the specific tendon. This study incorporated tendons classified as having energy-storing functions and positional functions; however, it should be noted that these two categories are not exhaustive and many tendons have unique physiological requirements that are not captured within this classification scheme.

Biochemical determination of elastin content in different tendons confirmed that tendons with an energy-storing function have greater elastin content [4], although unexpected differences between species were much greater than the differences between tendon types within individual species. The greater elastin content in human tendon is in agreement with previous results investigating elastin content and morphology in skin across multiple species, where human skin had the most elastin out of all species analyzed, which included pig, cow, dog, mouse, and many others [35]. It is possible that the unique joint geometry required for a bipedal gait places different requirements on the tendons of the human lower limb, requiring more elastin to properly function. In addition, hu-

man is the only species of those analyzed whose lifespan exceeds the half-life of elastin [36]. Since elastin begins to degrade in late age in humans, it is possible that more elastin is produced during development in order to compensate for the elastin lost later in life. Further quantification of elastin content in additional species, particular ones with bipedal gait and with longer lifespans, would help evaluate these hypotheses.

The comprehensive analysis of the morphology of the elastic fiber network in tendon particularly highlights the difference between the IFM and the FM with detail not previously achieved. In agreement with past studies, tendon IFM has more elastin than the FM [3,4]. However, this distinction between FM and IFM was greater in energy-storing tendon and did not reach statistical significance in positional tendon. In addition to a difference in elastin volume, the elastic fiber network in the IFM was less aligned and more connected than the elastic fibers in the FM across all tendons. The conclusion from this thorough analysis of the elastic fiber morphology matches previous qualitative observations of a more mesh-like elastic fiber network in the IFM as well as more basic quantitative approaches [3,4]. Moreover, the IFM had a four-fold greater volume of cell nuclei compared to the FM.

Differences in the elastic fiber network between tendon types and between species were more limited. In general agreement with the biochemical data, analysis of 3D image stacks from two-photon microscopy showed that energy-storing tendons had overall greater elastin volume than positional tendons. However, the distinction between tendon types was greater in the IFM where energy-storing tendons had high elastin volumes. Within the FM, energy-storing tendons did have more elastin compared to positional tendons, but the effect was not statistically significant. These data suggest that the bulk of differences in the contribution of elastin between tendon types lies within the IFM, in agreement with previous studies [37,38]. There were no significant species effects on elastin volume from the microscopy images, but the general trends did follow those seen in the protein quantification data. The only other tendon type effect was limited to cow tendon, where positional tendon showed less connected elastic fibers than in energy-storing tendons. Additionally, cow tendon had more aligned elastic fibers than the other species. These differences between cow tendon and mouse and human tendon may be a result of using different anatomical tendons from these species for this study. Although the selected tendons had similar functional requirements, anatomical differences may still account for some differences in the elastic fiber network.

Mechanical testing using elastase and control solutions, along with detailed statistical modeling, allowed isolation of the effects of elastin degradation on tendon mechanics. Overall, the properties dictating the elastic stress response of the tendon (i.e., *A, B*, modulus, transition stress and strain) were affected by elastin degradation across all tendon types and species without distinction (Fig. 9). The lone exception is transition strain, where the isolated elastase effect was only significant in human tendon, although differences in the elastase effect between species were not significant. The decrease in the material constant *A* corresponded to the decrease in modulus, where overall lower stress values led to a decreased slope of the loading curve. Similarly, the increase in the material constant *B* corresponded to increased transition strain and decreased transition stress, where the increased modulus gradient of the loading curve slightly shifted the measured transition point. The lack of variation of elastin degradation on these elastic properties despite differences in elastin content suggests that there may be a low threshold for elastin quantity that is necessary to maintain native elastic properties, yet additional elastin content above that threshold does not produce additional changes to the elastic stress response of tendon.

On the other hand, changes to the viscoelastic properties were not universal among species or tendon types. The constant *C* from fitting the stress relaxation data was increased after elastin degradation only in human tendon, indicating that elastin functions to maintain stress when the tendon is held for a period of time at a fixed strain. Conversely, the effect of elastase on the slow relaxation time constant τ_2 did not differ by species, but rather by tendon type. Elastin degradation decreased τ_2 only in energy-storing tendons, which indicates that equilibrium stress was reached more quickly. These effects on stress relaxation seem to be related to differences in elastin content between tendon types and species: the greater elastin content in energy-storing tendon compared to positional influences the rate of relaxation, while the larger difference in elastin content between species affects the magnitude of relaxation. In addition, hysteresis values were increased by elastin degradation only in mouse energy-storing tendon, although there is no clear basis in elastin content or structure to account for this effect. Because hysteresis typically increases at larger strains and stresses [13], it is possible that hysteresis measurements were also impacted by the decreased stresses in the post-incubation tests which then masked the effect of elastase on hysteresis in some tendon types or species.

Interestingly, there were no major differences in the response to elastin degradation between mouse tendon compared to cow and human tendon, as would be expected if the elastic fibers in the IFM played a significant role in tendon mechanics. Therefore, these data suggest that the interfascicular elastic fibers are not active in maintaining mechanical properties under a purely tensile loading regime. This result is not unexpected if the tendon fascicles are continuous across the whole gauge length of the clamped tendon. However, the type of loading experienced by tendons *in vivo* is seldomly as simple as loading during experimental testing. Tendons often wrap around bony structures that act as pulleys or are impinged upon by other tissues adjacent to the tendon, thus subjecting the tendon to complex multiaxial loading [39,40]. Even regions of tendons with a clear path can experience heterogeneous strain and corresponding shear between tendon sub-units [41–43]. Elastic fibers in the IFM may therefore still be integral to the overall mechanical function of tendon despite not influencing purely tensile properties along the main axis of the tendon. In support of this, prior studies have shown elastase had a greater effect on shear and off-axis tensile properties compared to tensile loading along the primary axis of the tendon [16,19,20,44], and elastase treatment had major impacts on direct shear testing of isolated tendon IFM including a substantial loss to fatigue resistance [10]. Future work incorporating *in situ* testing to evaluate the heterogeneous tensile and shear strain experienced by tendon in its anatomical location would help to evaluate how tendon IFM is loaded during *in vivo* tendon use and how elastin in the IFM contributes to overall tendon function.

The results presented herein may initially seem to contradict previous results from our lab using elastinopathic mouse models (i.e., $Eln^{+/-}$ and $Fbln5^{-/-}$), where reduced elastin content or disconnected elastin led to increased tendon modulus [12,13]. However, it should be noted that these genetic mouse models represent a fundamentally different approach than the current study. While elastase testing measures the effect of elastin degradation in an initially normal tendon, elastinopathic mouse models evaluate how tendon is affected when developed in the absence of a complete and functional elastic fibers network. These models can be related to the clinical effects of elastin degradation that results from aging and elastinopathic heritable disorders, respectively. Moreover, the effects of elastase compared to those of the mouse models are not inconsistent when the different experimental approaches are considered. In this study, mechanical tests were limited to low strains (i.e., $\leq$6%) to avoid tissue damage because of the repeated me-

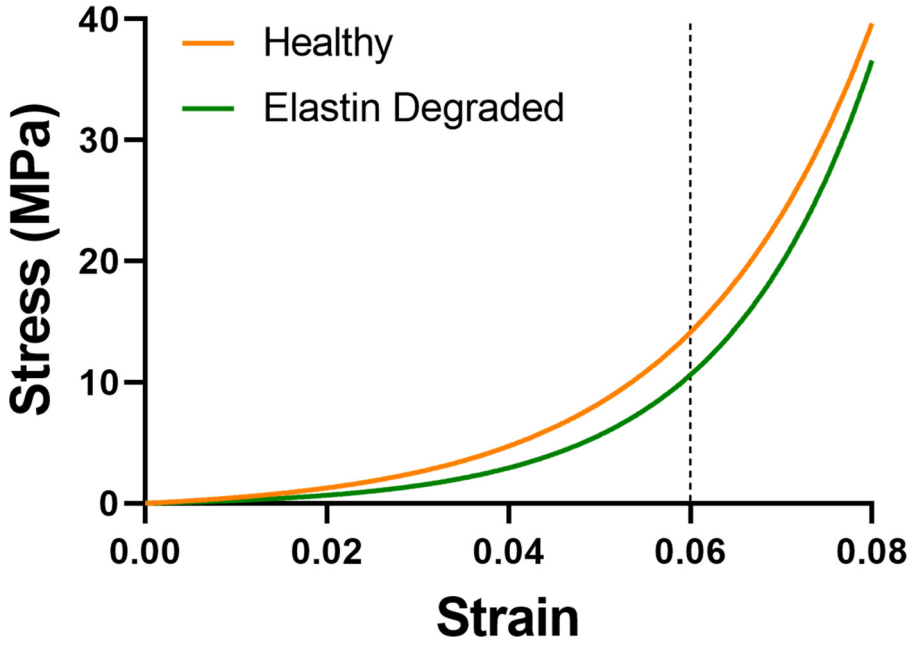

Fig. 9. Representation of the isolated effect of elastin degradation on the instantaneous elastic stress response of tendon using Eq. (1). The loading curve for "healthy" tendon uses values for *A* and *B* representative of a typical sample used in this study, while the "elastin degraded" loading curve uses values for *A* and *B* reflecting the changes in material properties caused by elastin degradation. The dashed vertical line represents the maximum strain used for experimental testing in this study; curves to the right of the dashed line are extrapolated. At lower strains, tendon with degraded elastin has lower stresses and a shifted transition point. At higher strains, stresses in the elastin degraded tendon increase more rapidly due to the increased modulus gradient of the stress-strain curve.

chanical testing approach and to represent physiologically relevant strain values [45]. The modulus measured in this study was determined by linear fitting to stress data between 5.5 and 6% strain; it is likely that the slope of the stress-strain curves would continue to increase at greater strain magnitudes, especially after elastase treatment where the transition point is shifted. Therefore, the decreased modulus observed following elastase treatment does not necessarily indicate that the modulus at higher strains would also be decreased. Moreover, the increased modulus gradient which also resulted from elastin degradation suggests that the modulus of elastase-treated samples could eventually match or exceed control samples at increasing strains. However, the exponential assumption for the shape of the stress-strain curve is less applicable at higher strains when the curve becomes more linear, so this extrapolation should be interpreted with caution (Fig. 9). Supporting this hypothesis, prior research that performed tensile testing to failure of ligament treated with elastase demonstrated a non-significant increase in failure modulus in elastase-treated ligaments compared to controls [16]. The increase in modulus at higher strains could be a result of less collagen regulation due to elastin degradation, which allows greater reorganization and higher alignment of collagen resulting from the decreased regulation of collagen engagement by elastic fibers. The overall stiffness of the tissue would then be increased due to the greater collagen alignment and engagement.

Differences in the effects on the transition point between these studies are similarly explained with differences in the experimental approach. In this study, the pre-stress was not reestablished for the post-incubation test, so the zero-strain state was referenced from the initial state of the tendon before the pre-incubation test. In contrast, the pre-stress was established before each test in the experiments with the elastinopathic murine models. Relating this to tendon function, tendons generally carry a low stress *in situ* even when not actively in use. If elastin in tendon becomes degraded and that pre-stress in the "unloaded" state drops, it is unclear if or how the tissue may actively remodel to reestablish that pre-stress in response to the elastin degradation. In the event that the tendon does not remodel, this could lead to greater tissue extensibility from the native state and overall increased joint laxity.

While biochemical quantification did demonstrate higher elastin content in energy-storing compared to positional tendon across all species, this difference had little mechanical impact on tendon; the only universal difference in the effect of elastin degradation between tendon types was a greater decrease in the long-time relaxation constant in energy-storing tendon. Microscopy data indicated that the bulk of the difference in elastin content stemmed from the IFM, and because these results suggest the IFM contributes little to purely tensile mechanics, the lack of mechanical differences between tendon types is appropriate. This largely agrees with prior research that indicated that the differences between tendon types arose from the IFM and not the FM [37]. Consequently, elastin may be more important in regulating shear or other off-axis properties of energy-storing compared to positional tendon due to IFM loading. Nonetheless, caution should still be taken when translating results between species or tendons, as there were some species-specific differences in these data and tendons can often defy a simplified binary classification scheme.

A limitation of this study is the non-specificity of elastase, which can degrade tissue constituents other than elastin. However, prior work has proven that fibrillar collagen is not targeted by elastase, and the proteoglycans that are targeted along with elastin do not significantly impact tensile tendon mechanics [10,15,46]. Therefore, it is reasonable to assume that changes to mechanical properties induced by elastase treatment are a result of elastin degradation. The large age range, and specifically the advanced age of human tendon donors used for biochemistry and mechanical testing, is another limitation of this study. This is unfortunately largely unavoidable due to the limited availability of younger human tendons, which are often reserved for allografts. An assump-

tion of this work is the functional analogy between the SDFT and LDET of the cow with the AT and TBAT of the mouse and human, respectively. While there are limitations to this approach because the tendon functions are not exactly the same between any of these tendons, both previous studies and the work presented herein demonstrate that many of the differences between the SDFT and LDET are also present between the AT and TBAT, warranting the placement of these tendons into the same general categories [11,13]. Additionally, the higher p-value significance threshold of 0.10 compared to the more commonly used value of 0.05 increases the risk of false positives in data analysis; however, this significance threshold adds more weight to the negative results in this study (i.e., what the effects of elastin degradation are not dependent on). Furthermore, few effects in this study had p-values between 0.05 and 0.10 and all the major conclusions of this study are based on effects where the p-value was less than 0.05.

In summary, elastin significantly affects the tensile elastic stress response of tendon across all species and tendon types. At low strains, elastin seems to bear a significant portion of the load while the underlying collagen architecture uncrimps and reorganizes. Extrapolating to larger strains when the collagen becomes more fully engaged, the modulus of elastin-degraded tendon may match or even potentially exceed native tissue due to the increased modulus gradient of the stress-strain curve. These results highlight the importance for elastin in tendon function across multiple tendon types and species, while providing further evidence for a more mechanistic understanding of how elastin regulates collagen engagement within fascicles to influence mechanical properties.

Funding

This work was supported by the National Science Foundation (1562107 and 2037125) and the National Institutes of Health (T32EB018266).

Declaration of Competing Interest

The authors declare that they have no known competing financial interests or personal relationships that could have appeared to influence the work reported in this paper.

Appendix A. Fitting quasi-linear viscoelastic theory to stress relaxation data

The quasi-linear viscoelastic theory describes the stress response over time as the convolution integral of the reduced relaxation function ($G(t)$) with the instantaneous elastic stress response ($\sigma^e(\varepsilon)$), as shown in Eq. (A1) [28].

$$\sigma(t) = \int_{-\infty}^{t} G(t-\tau)\frac{\delta\sigma^e(\varepsilon)}{\delta\varepsilon}\frac{\delta\varepsilon}{\delta\tau}\delta\tau \tag{A.1}$$

There have been multiple forms of the equations for the elastic stress response and the reduced relaxation function proposed to fit the model to data from soft tissue. In this study we adopted the commonly used forms [29–31]

$$\sigma^e(\varepsilon) = A\left(e^{B\varepsilon} - 1\right) \tag{A.2}$$

$$G(t) = \frac{1 + C[E_1(t/\tau_2) - E_1(t/\tau_1)]}{1 + C\ln(\tau_2/\tau_1)} \tag{A.3}$$

where E_1 is the exponential integral. The material constants A and B in the instantaneous elastic stress response describe the magnitude and modulus gradient of the loading curve, respectively. In the reduced relaxation function, the material constant C describes the shape of the relaxation curve while the time constants τ_1 and τ_2 describe how quickly the tissue relaxes over time.

Using the above forms for the instantaneous elastic response and the reduced relaxation function, the stress as a function of time during the ramp and the relaxation portion of the stress relaxation experiment is given in Eq. (A.4),

$$\sigma(t) = \begin{cases} \frac{AB\gamma}{1+C\ln(\tau_2/\tau_1)}\int_0^t \left\{1 + C\left(\frac{E_1[t-\tau]}{\tau_2} - \frac{E_1[t-\tau]}{\tau_1}\right)\right\}e^{B\gamma\tau}\delta\tau, & 0 < t < t_0 \\ \frac{AB\gamma}{1+C\ln(\tau_2/\tau_1)}\int_0^{t_0} \left\{1 + C\left(\frac{E_1[t-\tau]}{\tau_2} - \frac{E_1[t-\tau]}{\tau_1}\right)\right\}e^{B\gamma\tau}\delta\tau, & t \geq t_0 \end{cases} \tag{A.4}$$

where γ is the strain rate applied from $t = 0$ to $t = t_0$, and t_0 is the time when the target strain is reached [29].

For the purpose of fitting experimental data to the model, both the data and Eq. (A.4) can be normalized to the stress at $t = t_0$ [29]. This simplifies the model fitting by removing the material constant A from the equation.

$$\frac{\sigma(t)}{\sigma(t_0)} = \begin{cases} \frac{\int_0^t \left\{1+C\left(\frac{E_1[t-\tau]}{\tau_2} - \frac{E_1[t-\tau]}{\tau_1}\right)\right\}e^{B\gamma\tau}\delta\tau}{\int_0^{t_0} \left\{1+C\left(\frac{E_1[t_0-\tau]}{\tau_2} - \frac{E_1[t_0-\tau]}{\tau_1}\right)\right\}e^{B\gamma\tau}\delta\tau}, & 0 < t < t_0 \\ \frac{\int_0^{t_0} \left\{1+C\left(\frac{E_1[t-\tau]}{\tau_2} - \frac{E_1[t-\tau]}{\tau_1}\right)\right\}e^{B\gamma\tau}\delta\tau}{\int_0^{t_0} \left\{1+C\left(\frac{E_1[t_0-\tau]}{\tau_2} - \frac{E_1[t_0-\tau]}{\tau_1}\right)\right\}e^{B\gamma\tau}\delta\tau}, & t \geq t_0 \end{cases} \tag{A.5}$$

The experimental data can then be fit to the model by minimizing the sum of squares error between the experimental data and the model predicted values to determine the material constants B, C, τ_1, and τ_2 [30]. This is shown in Eq. (A.6),

$$\min_{B,C,\tau_1,\tau_2} \sum_i \left[\frac{S_i}{S_0} - \frac{\sigma(t_i)}{\sigma(t_0)}\right]^2 \tag{A.6}$$

where the experimental data is defined as (t_i, S_i), and S_0 is the experimental peak stress. The minimization was performed with initial guesses for B, C, τ_1, and τ_2 based on preliminary data, and the initial guess was multiplied by a random factor between 0.1 and 10 for each fitting [30].

However, this approach did not converge to a global minimum for all experimental data; therefore, a modification to the approach was necessary. For data where the minimization did not converge, C and τ_2 were observed to increase in tandem by several orders of magnitude without meaningfully changing the goodness of fit. Consequently, the minimization was changed to the following form:

$$\min_{\tau_2}\left\{C\left(\min_{B,C,\tau_1}\sum_i\left[\frac{S_i}{S_0} - \frac{\sigma(t_i)}{\sigma(t_0)}\right]^2\right)\right\}. \tag{A.7}$$

This approach was implemented by performing the inner minimization using the interior-point algorithm one hundred times at different fixed τ_2 values randomly selected on a logarithmic scale between 10^2 and 10^6, while initial guesses for B, C, and τ_1 for each iteration were generated as described above [32]. The experimental data was downsampled to increase the speed of the interior-point algorithm. Out of those one hundred potential fits, the final fit was selected such that the product of C and the sum of squares error was minimized. This modified approach converged to a global minimum with a good fit to the experimental data for all samples.

After the values for B, C, τ_1, and τ_2 were determined using eq. A.7, the material constant A was calculated as follows:

$$A = \sigma(t_0)\frac{1 + C\ln(\tau_2/\tau_1)}{B\gamma\int_0^{t_0}\left\{1 + C\left(\frac{E_1[t_0-\tau]}{\tau_2} - \frac{E_1[t_0-\tau]}{\tau_1}\right)\right\}e^{B\gamma\tau}\delta\tau}. \tag{A.8}$$

Appendix B: Effect of species and tendon type on baseline mechanical properties

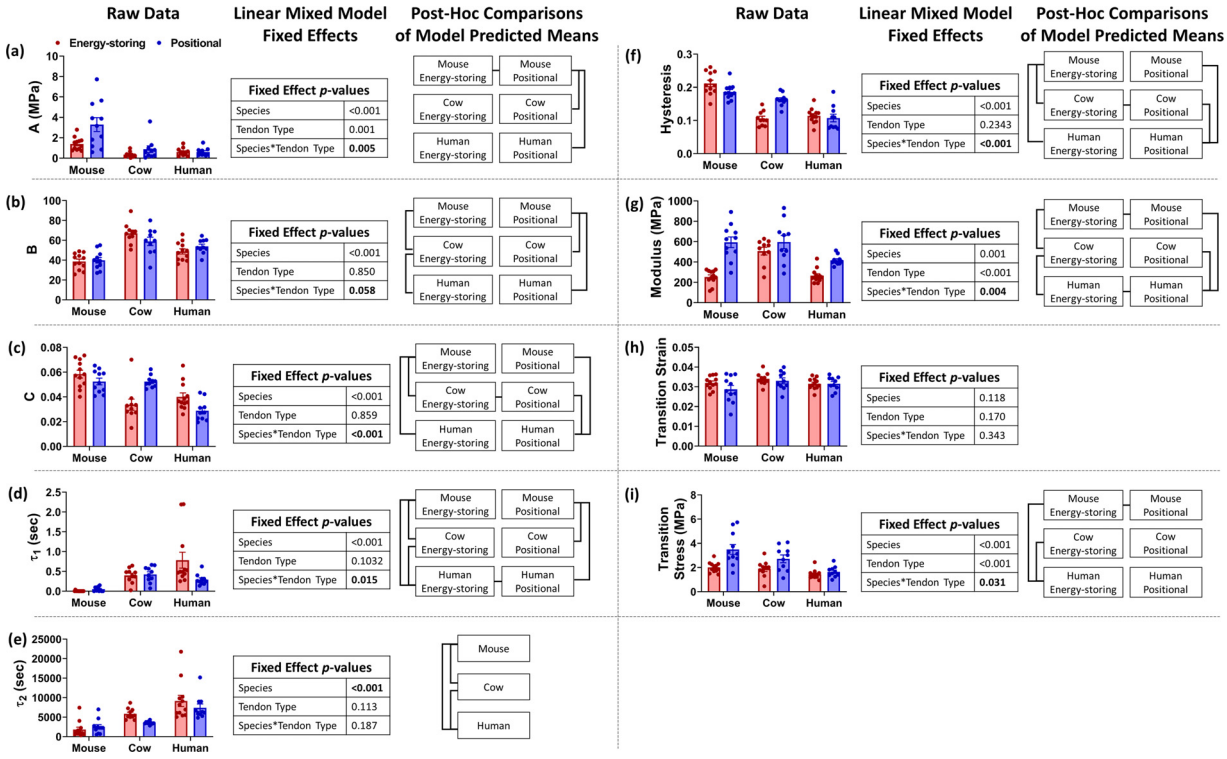

Fig. B1. Data and statistical analysis of baseline mechanical data across species and tendon types. Connecting lines between groups show significant differences in post-hoc testing ($p < 0.1$).

References

[1] A.K. Baldwin, A. Simpson, R. Steer, S.A. Cain, C.M. Kielty, Elastic fibres in health and disease, Expert Rev. Mol. Med. 15 (2013) 1–30, doi:10.1017/erm.2013.9.

[2] X. Pang, J.P. Wu, G.T. Allison, J. Xu, J. Rubenson, M.-H. Zheng, D.G. Lloyd, B. Gardiner, A. Wang, T.B. Kirk, Three dimensional microstructural network of elastin, collagen, and cells in Achilles tendons, J. Orthop. Res. 35 (2017) 1203–1214, doi:10.1002/jor.23240.

[3] T.M. Grant, M.S. Thompson, J. Urban, J. Yu, Elastic fibres are broadly distributed in tendon and highly localized around tenocytes, J. Anat. 222 (2013) 573–579, doi:10.1111/joa.12048.

[4] M.S.C. Godinho, C.T. Thorpe, S.E. Greenwald, H.R.C. Screen, Elastin is localised to the interfascicular matrix of energy storing tendons and becomes increasingly disorganised with ageing, Sci. Rep. 7 (2017) 9713, doi:10.1038/s41598-017-09995-4.

[5] J.R. Hill, J.D. Eekhoff, R.H. Brophy, S.P. Lake, Elastic fibers in orthopedics: Form and function in tendons and ligaments, clinical implications, and future directions, J. Orthop. Res. (2020) 24695, doi:10.1002/jor.24695.

[6] E.D. Shirley, P.D. Sponseller, Marfan syndrome, J. Am. Acad. Orthop. Surg. (2009), doi:10.5435/00124635-200909000-00004.

[7] B.R. Pober, Williams-beuren syndrome, N. Engl. J. Med. (2010), doi:10.1056/nejmra0903074.

[8] N.O. Sakati, W.L. Nyhan, C.S. Shear, Syndrome of cutis laxa, ligamentous laxity, and delayed development, Pediatrics 72 (1983) 850–856.

[9] D.A.D. Parry, A.S. Craig, G.R.G. Barnes, Tendon and ligament from the horse: an ultrastructural study of collagen fibrils and elastic fibres as a function of age, Proc. R. Soc. Lond. Ser. B Biol. Sci. 203 (1978) 293–303, doi:10.1098/rspb.1978.0106.

[10] M.S. Godinho, C.T. Thorpe, S.E. Greenwald, H.R.C. Screen, Elastase treatment of tendon specifically impacts the mechanical properties of the interfascicular matrix, Acta Biomater. 123 (2021) 187–196, doi:10.1016/j.actbio.2021.01.030.

[11] D. Patel, D.E. Zamboulis, E.M. Spiesz, H.L. Birch, P.D. Clegg, C.T. Thorpe, H.R.C. Screen, Structure-function specialisation of the interfascicular matrix in the human achilles tendon, Acta Biomater. 131 (2021) 381–390, doi:10.1016/j.actbio.2021.07.019.

[12] J.D. Eekhoff, F. Fang, L.G. Kahan, G. Espinosa, A.J. Cocciolone, J.E. Wagenseil, R.P. Mecham, S.P. Lake, Functionally distinct tendons from elastin haploinsufficient mice exhibit mild stiffening and tendon-specific structural alteration, J. Biomech. Eng. 139 (2017) 111003, doi:10.1115/1.4037932.

[13] J.D. Eekhoff, H. Steenbock, I.M. Berke, J. Brinckmann, H. Yanagisawa, J.E. Wagenseil, S.P. Lake, Dysregulated assembly of elastic fibers in fibulin-5 knockout mice results in a tendon-specific increase in elastic modulus, J. Mech. Behav. Biomed. Mater. 113 (2021) 104134, doi:10.1016/j.jmbbm.2020.104134.

[14] R.M. Alexander, Energy-saving mechanisms in walking and running, J. Exp. Biol. 160 (1991) 55–69.

[15] T.M. Grant, C. Yapp, Q. Chen, J.T. Czernuszka, M.S. Thompson, The mechanical, structural, and compositional changes of tendon exposed to elastase, Ann. Biomed. Eng. 43 (2015) 2477–2486, doi:10.1007/s10439-015-1308-5.

[16] H.B. Henninger, C.J. Underwood, S.J. Romney, G.L. Davis, J.A. Weiss, Effect of elastin digestion on the quasi-static tensile response of medial collateral ligament, J. Orthop. Res. 31 (2013) 1226–1233, doi:10.1002/jor.22352.

[17] H. Millesi, R. Reihsner, G. Hamilton, R. Mallinger, E.J. Menzel, Biomechanical properties of normal tendons, normal palmar aponeuroses and palmar aponeuroses from patients with dupuytren's disease subjected to elastase and chondroitinase treatment, Connect. Tissue Res. (1995), doi:10.3109/03008209509028398.

[18] A. Svärd, M. Hammerman, P. Eliasson, Elastin levels are higher in healing tendons than in intact tendons and influence tissue compliance, FASEB J. 34 (2020) 13409–13418, doi:10.1096/fj.202001255R.

[19] F. Fang, S.P. Lake, Multiscale mechanical integrity of human supraspinatus tendon in shear after elastin depletion, J. Mech. Behav. Biomed. Mater. 63 (2016) 443–455, doi:10.1016/j.jmbbm.2016.06.032.

[20] H.B. Henninger, W.R. Valdez, S.A. Scott, J.A. Weiss, Elastin governs the mechanical response of medial collateral ligament under shear and transverse tensile loading, Acta Biomater. 25 (2015) 304–312, doi:10.1016/j.actbio.2015.07.011.

[21] A.H. Lee, D.M. Elliott, Multi - scale loading and damage mechanisms of plantaris and rat tail tendons, J. Orthop. Res. 37 (2019) 1827–1837, doi:10.1002/jor.24309.

[22] H.L. Birch, Tendon matrix composition and turnover in relation to functional requirements, Int. J. Exp. Pathol. 88 (2007) 241–248, doi:10.1111/j.1365-2613.2007.00552.x.

[23] I. Stoilov, B.C. Starcher, R.P. Mecham, T.J. Broekelmann, Measurement of elastin, collagen, and total protein levels in tissues, in: Methods in Cell Biology, 1st ed., Elsevier Inc., 2018, pp. 133–146, doi:10.1016/bs.mcb.2017.08.008.

[24] Z. Shen, Z. Lu, P.Y. Chhatbar, P. O'Herron, P. Kara, An artery-specific fluorescent dye for studying neurovascular coupling, Nat. Methods 9 (2012) 273–276, doi:10.1038/nmeth.1857.
[25] M.T. Ke, S. Fujimoto, T. Imai, SeeDB: a simple and morphology-preserving optical clearing agent for neuronal circuit reconstruction, Nat. Neurosci. 16 (2013) 1154–1161, doi:10.1038/nn.3447.
[26] J.D. Eekhoff, S.P. Lake, Three-dimensional computation of fibre orientation, diameter and branching in segmented image stacks of fibrous networks, J. R. Soc. Interface 17 (2020) 20200371, doi:10.1098/rsif.2020.0371.
[27] J. Bieth, B. Spiess, C.G. Wermuth, The synthesis and analytical use of a highly sensitive and convenient substrate of elastase, Biochem. Med. 11 (1974) 350–357, doi:10.1016/0006-2944(74)90134-3.
[28] Y.C. Fung, R. Skalak, Biomechanics: mechanical properties of living tissues, J. Biomech. Eng. 103 (1981), doi:10.1115/1.3138285.
[29] M.K. Kwan, T.H.C. Lin, S.L.Y. Woo, On the viscoelastic properties of the anteromedial bundle of the anterior cruciate ligament, J. Biomech. 26 (1993) 447–452, doi:10.1016/0021-9290(93)90008-3.
[30] S.D. Abramowitch, S.L.Y. Woo, An improved method to analyze the stress relaxation of ligaments following a finite ramp time based on the quasi-linear viscoelastic theory, J. Biomech. Eng. 126 (2004) 92–97, doi:10.1115/1.1645528.
[31] R.M. Castile, N.W. Skelley, B. Babaei, R.H. Brophy, S.P. Lake, Microstructural properties and mechanics vary between bundles of the human anterior cruciate ligament during stress-relaxation, J. Biomech. 49 (2016) 87–93, doi:10.1016/j.jbiomech.2015.11.016.
[32] R.H. Byrd, M.E. Hribar, J. Nocedal, An interior point algorithm for large-scale nonlinear programming, SIAM J. Optim. 9 (1999) 877–900, doi:10.1137/S1052623497325107.
[33] R.L. Wasserstein, N.A. Lazar, The ASA statement on p -values: context, process, and purpose, Am. Stat. 70 (2016) 129–133, doi:10.1080/00031305.2016.1154108.
[34] C. Andrade, The P value and statistical significance: misunderstandings, explanations, challenges, and alternatives, Indian J. Psychol. Med. 41 (2019) 210–215, doi:10.4103/IJPSYM.IJPSYM_193_19.
[35] B. Starcher, R.L. Aycock, C.H. Hill, Multiple roles for elastic fibers in the skin, J. Histochem. Cytochem. 53 (2005) 431–443, doi:10.1369/jhc.4A6484.2005.
[36] S.D. Shapiro, S.K. Endicott, M.A. Province, J.A. Pierce, E.J. Campbell, Marked longevity of human lung parenchymal elastic fibers deduced from prevalence of D-aspartate and nuclear weapons-related radiocarbon, J. Clin. Invest. 87 (1991) 1828–1834, doi:10.1172/JCI115204.
[37] C.T. Thorpe, C.P. Udeze, H.L. Birch, P.D. Clegg, H.R.C. Screen, Specialization of tendon mechanical properties results from interfascicular differences, J. R. Soc. Interface 9 (2012) 3108–3117, doi:10.1098/rsif.2012.0362.
[38] C.T. Thorpe, M.S.C. Godinho, G.P. Riley, H.L. Birch, P.D. Clegg, H.R.C. Screen, The interfascicular matrix enables fascicle sliding and recovery in tendon, and behaves more elastically in energy storing tendons, J. Mech. Behav. Biomed. Mater. 52 (2015) 85–94, doi:10.1016/j.jmbbm.2015.04.009.
[39] I. Bah, N.R.J. Fernandes, R.L. Chimenti, J. Ketz, A.S. Flemister, M.R. Buckley, Tensile mechanical changes in the Achilles tendon due to insertional achilles tendinopathy, J. Mech. Behav. Biomed. Mater. 112 (2020) 104031, doi:10.1016/j.jmbbm.2020.104031.
[40] F. Fang, S.P. Lake, Multiscale strain analysis of tendon subjected to shear and compression demonstrates strain attenuation, fiber sliding, and reorganization, J. Orthop. Res. 33 (2015) 1704–1712, doi:10.1002/jor.22955.
[41] S. Bogaerts, C. De Brito Carvalho, L. Scheys, K. Desloovere, J. D'hooge, F. Maes, P. Suetens, K. Peers, Evaluation of tissue displacement and regional strain in the Achilles tendon using quantitative high-frequency ultrasound, PLoS One 12 (2017) 1–16, doi:10.1371/journal.pone.0181364.
[42] J. Bojsen-Møller, S.P. Magnusson, Heterogeneous loading of the human Achilles tendon *in vivo*, Exerc. Sport Sci. Rev. 43 (2015) 190–197, doi:10.1249/JES.0000000000000062.
[43] C. Lersch, A. Grötsch, B. Segesser, J. Koebke, G.P. Brüggemann, W. Potthast, Influence of calcaneus angle and muscle forces on strain distribution in the human Achilles tendon, Clin. Biomech. 27 (2012) 955–961, doi:10.1016/j.clinbiomech.2012.07.001.
[44] H.B. Henninger, B.J. Ellis, S.A. Scott, J.A. Weiss, Contributions of elastic fibers, collagen, and extracellular matrix to the multiaxial mechanics of ligament, J. Mech. Behav. Biomed. Mater. 99 (2019) 118–126, doi:10.1016/j.jmbbm.2019.07.018.
[45] M. Ryan, R. Barrett, Using digital image correlation to examine in-vivo localised Achilles tendon strain, J. Sci. Med. Sport 18 (2014) e57–e58, doi:10.1016/j.jsams.2014.11.275.
[46] F. Fang, S.P. Lake, Multiscale mechanical evaluation of human supraspinatus tendon under shear loading after glycosaminoglycan reduction, J. Biomech. Eng. 139 (2017) 1–8, doi:10.1115/1.4036602.